Preparation of electrospun magnetic polyvinylbutyral/Fe_2O_3 nanofibrous membranes for effective removal of iron ions from groundwater

Petra Peer [1], Martin Cvek [2], Michal Urbanek [2] and Michal Sedlacik [2,3]

[1]Institute of Hydrodynamics of the Czech Academy of Sciences, Pod Patankou 5, 166 12 Prague 6, Czech Republic

[2]Centre of Polymer Systems, University Institute, Tomas Bata University in Zlin, Trida T. Bati 5678, 760 01 Zlin, Czech Republic

[3]Department of Production Engineering, Faculty of Technology, Tomas Bata University in Zlin, Vavreckova 275, 760 01 Zlin, Czech Republic

Correspondence to: Petra Peer (E-mail: peer@ih.cas.cz)

ABSTRACT

Removing iron ions from groundwater to purify it is a challenge faced by countries across the globe, which is why developing polymeric microfiltration membranes has garnered much attention. The authors of this study set out to develop nanofibrous membranes by embedding magnetic Fe_2O_3 nanoparticles (MNPs) into polyvinylbutyral (PVB) nanofibres via the electrospinning process. Investigation was made into the effects of the concentration of the PVB and MNPs on the morphology of the nanofibres, their magnetic properties and capacity for filtration to remove iron ions. The fabrication and presence of well-incorporated MNPs in the PVB nanofibres were confirmed by scanning electron microscopy and transmission electron microscopy. Depending on the concentration of the MNPs, the membranes exhibited magnetization to the extent of 45.5 emu g^{-1}; hence, they exceeded the performance of related nanofibrous membranes in the literature. The magnetic membranes possessed significantly higher efficiency for filtration compared to their non-magnetic analogues, revealing their potential for groundwater treatment applications.

INTRODUCTION

In recent years, a great deal of interest has been shown in magnetoactive polymeric fibrous membranes, since their properties are influenced by the presence of an externally applied magnetic field. Electrospun nanofibrous membranes containing an amount of magnetic iron oxide nanoparticles have become a necessary material for various uses, including tissue engineering, sensors, wound dressings, magnetic hyperthermia therapy and wastewater treatment.[1-7] It is possible to incorporate magnetic nanoparticles (MNPs) into a nanofibrous membrane in three different ways: (i) by utilizing pre-synthesized MNPs prior to electrospinning; (ii) treating the MNPs after the electrospinning process; or (iii) by utilizing in-situ synthesized MNPs. Novel magnetoactive microfibres were prepared with pre-formed iron oxide nanoparticles coated in oleic acid, which displayed superparamagnetic behaviour and proved stable in

aqueous media, making them potentially suitable for environmental applications.[8] The post-treated method was employed on a number of different nanofibrous membranes with iron oxide nanoparticles for subsequent treatment of toxic environmental pollutants.[9] Meanwhile, a single-stage, in-situ synthesis technique, was employed, whereby iron oxide nanoparticles were reduced during the electrospinning of poly(ethylene oxide) nanofibres.[10]

Attention has recently shifted to developing nanofibrous membranes for direct filtration. This stems from the fact that an electrospun nanofibrous non-woven textile can be applied as a selective layer for fabricating membranes for ultrafiltration, nanofiltration or even reverse osmosis. The efficiency of such filtration relates to pore size, porosity, surface energy and wettability.[11-15] Nevertheless, the requirements of a given nanofibrous membrane depend on the intended purpose - filtration of a particular liquid (wastewater, oil and water, salty water), or the potential to filter out microorganisms, heavy metals, particulates and chemicals.[16] A suitable technique for improving the performance of filtration was found to be surface modification. Incorporating MNPs into the filter aided recovery of the membranes after the oil-in-water sorption process.[17] Superparamagnetic nanofibres were developed that produced active hydroxyl radicals, under light irradiation, for applications involving photocatalysis in water purification.[18] In another study, authors demonstrated that a functionalized magnetic nanofibrous composite could effectively remove chromium (VI) adsorbents from water.[19]

In addition to other heavy metals, the presence of iron in groundwater is an issue affecting countries across the world.[20] Although iron generally does not present a danger to human health or the environment, it has the potential to cause serious problems, especially at high levels of contamination. Above certain levels, complications ensue in water related to aesthetic and organoleptic aspects, including discolouration, high turbidity and a metallic taste, making it unpleasant for consumption. If people consume excessive concentrations, it can even prove life-threatening, possibly causing cardiomyopathy, endocrine, neurodegenerative and other disorders.[21] From a technical point of view, operational problems arise as a consequence of excess iron, such as pipelines becoming blocked and the possibility of clogging.[22] In a response to these alerts, directives from the World Health Organization and European Commission recommend that the concentration of iron ions in drinking water should be less than 0.3 mg l^{-1} and 0.2 mg l^{-1}, respectively.[20] Several technologies have been introduced to eliminate iron contaminants from water, including the use of membranes, electrocoagulation, chemical precipitation, ion exchange and an adsorption process.[22] Membrane filtration technologies are particularly effective due to the structural advantages and functionalization of the nanofibres therein. For instance, a novel multifunctional cellulose acetate membrane with chitin nanocrystals reported in the literature exhibited good mechanical properties and significantly reduced the extent of biofouling, in addition to which a biofilm was successfully fabricated.[23]

Herein, study was made as to the effect exerted by concentrations of the PVB and MNPs on the rheological properties of solutions and the morphological and magnetic parameters of the resultant electrospun nanofibrous PVB membranes. Filtration experiments were performed without the external magnetic field to determine their potential for implementation in real-world conditions. Since the components utilized were obtained from commercial sources, large-scale production of such membranes would be feasible. The PVB comprising the polymeric part of the material was environment-friendly, non-toxic and odourless,

and is frequently added to solutions to improve spinnability.[24] Based on the results discerned, certain types of the magnetic nanofibrous membrane could constitute part of a filter for water purification purposes.

EXPERIMENTAL

Polyvinyl butyral (Mw = 60,000 g mol^{-1}; Mowital B 60H; provided by Kuraray Specialities Europe, Germany) was dissolved in methanol (PENTA; at the quality of p.a.; Czech Republic) at four different concentrations (6, 8, 10 and 12 wt%). According to the data sheet from the supplier, the structure of Mowital B 60H comprised vinyl butyral, vinyl alcohol and vinyl acetate; herein at 75–81, 18–21 and 1– 4 %, respectively. Magnetic nanoparticles (MNPs), consisting of iron (III) oxide, produced by NanoArc (Germany), were mixed with the PVB solution at the concentrations of 1, 5, 10, 15, and 20 wt%. The size of the MNPs ranged between 20–40 nm, their surface areas equalling 30–60 m^2 g^{-1}. Ferric sulphate hydrate, $Fe_2(SO_4)_3 \cdot 9H_2O$ (Analytika, Czech Republic), was dissolved in distilled water for the model metal solution.

The polymer solution was homogenized on a magnetic stirrer set to 250 rpm at 25°C for 48 hours. Subsequently, the MNPs were added into the polymer solution and mixed mechanically for 5 minutes; the concentrations applied to prepare the series of PVB and PVB/MNPs solutions are summarized in Table 1.

TABLE 1 Concentrations of the polymer solution and MNPs utilized for preparing the PVB and PVB/MNPs solutions in methanol.

Sample code	PVB concentration [wt%]	MNP concentration [wt%]
PVB6	6	-
PVB8	8	-
PVB10	10	-
PVB12	12	-
PVB6/MNP5	6	5
PVB8/MNP5	8	5
PVB10/MNP5	10	5
PVB12/MNP5	12	5
PVB8/MNP1	8	1
PVB8/MNP10	8	10
PVB8/MNP15	8	15
PVB8/MNP20	8	20

Rheological measurement of the polymer solutions was performed in rotational and oscillatory mode on a Physica MCR 501 device (Anton Paar, Austria), equipped with concentric cylinders (26.6/28.9 mm inner/outer diameters) at a constant temperature of 25°C. The steady shear values for the polymer solutions were gauged across a range of shear rates from 0.01 to 300 s^{-1}. Oscillatory shear measurements were taken at strain within a linear viscoelasticity region (1%) at frequencies ranging from 0.1 to 100 Hz. In order to process the oscillatory data, the loss factor tan δ (phase angle δ) was calculated by the following Equation (1):

$$\tan \delta = \frac{G''}{G'} , \quad (1)$$

where *G*'' is the loss (viscous) modulus and *G*' is the storage (elastic) modulus.

The nanofibrous membranes were spun on a custom-built laboratory device that consisted of a high voltage power supply (Spellman SL70PN150, USA), a carbon steel stick (10 mm in diameter) and a motionless flat metal collector. The electrospinning process was carried out at a fixed voltage of 20 kV, while the tip-to-collector distance was set to 100 mm. The experiments were carried out under ambient conditions (temperature 21±1°C, relative humidity 52±1%). A fixed volume (1 ml) of each polymer solution with or without the MNPs was placed on the tip of the apparatus and electrospun for a different period of time, according to the concentration of MNPs.

The morphology of the nanofibrous membranes prepared on aluminium foil was characterized on a Vega 3, high-resolution scanning electron microscope (Tescan, Czech Republic). Prior to imaging, a conductive layer was sputtered onto the samples. The mean diameter of the fibres was determined with the aid of Adobe Creative Suite software, in which 300 fibres were analysed from 3 different images. The data were examined by conducting a one-way ANOVA statistical test in Minitab software (version 14). The topology of the MNPs within the nanofibres was studied on a high-resolution transmission electron microscope, a JEOL unit (JEM 2100, Japan) fitted with an LaB6 cathode and operated at 80 kV. The fibres were inspected on SPI double-folding 100/200 copper grids.

Prior to such tests, the nanofibrous membranes had been removed carefully from the aluminium collector and subjected to analysis. Fourier-transform infra-red spectroscopy (FTIR) was performed at laboratory temperature on a Nicolet iS5 unit (Thermo Scientific, USA) equipped with the iD5 ATR accessory and a germanium crystal. The spectra were collected in a wavelength region from 4 000 to 800 cm^{-1} across 64 scans with a spectral resolution of 2 cm^{-1}.

The magnetic properties of the PVB nanofibrous membranes supplemented with the embedded MNPs were determined on a vibrating-sample magnetometer (VSM 7407, Lake Shore, USA), in a magnetic field ranging up to 14 kOe (~1150 kA/m) at laboratory temperature (23°C). The samples were carefully placed in the VSM sample holder (730931 Kel-F, bulk upper/bottom cup) coupled with a fibreglass (740935) sample tail. The amplitude of vibration, frequency of vibration and time constant were set to 1.5 mm, 82 Hz and 100 ms, respectively.

The wettability of the magnetic nanofibrous membranes electrospun on the aluminium foil was analysed by gauging their contact angles, in accordance with the sessile drop method on a Surface Energy Evaluation System by Advex Instruments (Czech Republic) at laboratory temperature. The final values were calculated as the arithmetic means of ten independent measurements. Deionized water was employed as the reference liquid; the volume of each deposited droplet equalled 3 µl.

Filtration experiments were conducted on selected PVB/MNP samples, which had been electrospun (thickness of layer = 20 µm) onto polypropylene (PP) non-woven textile (thickness = 210 µm). The latter possessed an applicable structure and adequate mechanical properties for the given purpose, its specifications comprising a fibre diameter of 4 µm, permeation flux of 95,000 l m^{-2} h^{-1} and porosity of 53%.

The permeation fluxes of the membranes were determined on a dead-end filtration system (Model GV 025/2, Whatman, Germany), set to a transmembrane pressure of 4 bar. Testing involved the use of both the deionized water and model metal solution (concentration of Fe(III) = 5 mg l^{-1}; pH = 4; temperature = 23°C). The Fe(III) concentrations of the permeate solution were gauged on an inductively coupled plasma optical emission spectrometer (ICP-OES, Thermo Fisher Scientific, USA). At least 3 permeate fluxes of water and model metal solutions were tested for the selected samples, and the average value for permeation flux (*F*) was calculated as follows:

$$F\ [\mathrm{L\ m^{-2}\ h^{-1}}] = \frac{V}{At}\ , \tag{2}$$

where *A* is the effective area of the filter membrane (m^2) and *V* is permeation volume (100 ml) over an interval *t* (h). Filtration efficiency (*FE*) was calculated by the following equation:

$$FE\ [\%] = \frac{C_0 - C_p}{C_0} \times 100\ , \tag{3}$$

where C_p and C_0 represent the concentrations of the permeation and feed solutions, respectively. The porosity (*P*) of the filter (consisting of the PP non-woven textile with nanofibrous membranes) was worked out via the gravimetric method and the following equation:

$$P\ [\%] = \frac{m_{wet} - m_d}{\rho_w A l} \times 100\ , \tag{4}$$

where m_{wet} is the weight of the wet membrane, m_d is the weight of the dry membrane, ρ_w is water density, *A* is the effective area of the membrane (*A* = 0.000314 m^2) and *l* is the thickness of the membrane. Deionized water was employed as the wetting liquid that penetrated into the pores of the filter. Pore size distribution was determined by image analysis of SEM micrographs (in Adobe Creative Suite software); the mean pore size was calculated from over 30 values.

RESULTS AND DISCUSSION

Rheological characterization

It is known that the intensity of the electrospinning process and diameters of the fibres are strongly influenced by the rheological parameters of the given solution, such as its viscosity, storage and loss moduli. If the polymer solution is too viscous and elastic in quality, then it proves unsuitable for electrospinning.[25] Upon rise in the viscosity of the polymer solution, the process slows down and the polymer jet is insufficiently drawn out, thereby increasing the diameter of the resultant fibre. Generally, the presence of an additive (herein, the MNPs) in the polymer solution increases viscosity and alters rheological behaviour.[26]

The shear viscosity of the neat PVB and PVB/MNPs solutions rose in line with higher polymer concentration, as shown in Figure 1a. The PVB solutions almost exhibited Newtonian behaviour independently at various polymer concentrations; hence, the elasticity of these samples was minimal (δ = 90°). However, when the MNPs were incorporated into the PVB solution, the viscosity of the polymer suspension increased, as illustrated in Figure 1b. The greater concentration of the MNPs in the solution

also transformed the Newtonian behaviour into non-Newtonian, meaning that shear thinning occurred at higher shear rates. As a result, the elasticity of the solutions went up, especially for the more concentrated PVB/MNPs solutions; as depicted in Figure 2. The low phase angle values suggested a strong elastic quality, caused by the network structure among the interconnected MNPs and polymer chains. This aspect was indicative of the complicated production of such highly concentrated PVB nanofibres via electrospinning.

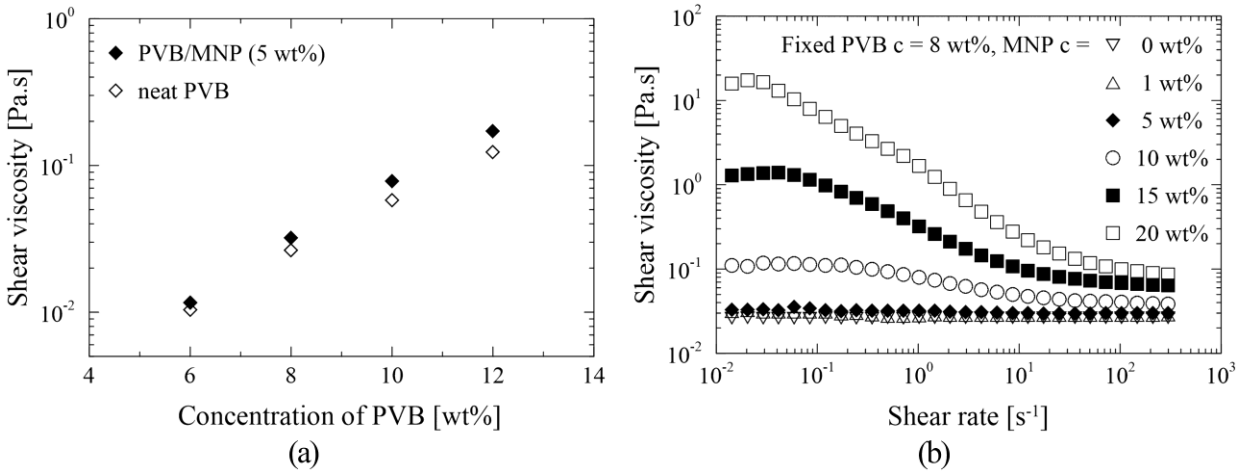

FIGURE 1 Rheological properties of the neat PVB and PVB/MNPs solutions: (a) effect of PVB concentration; (b) effect of MNP concentration.

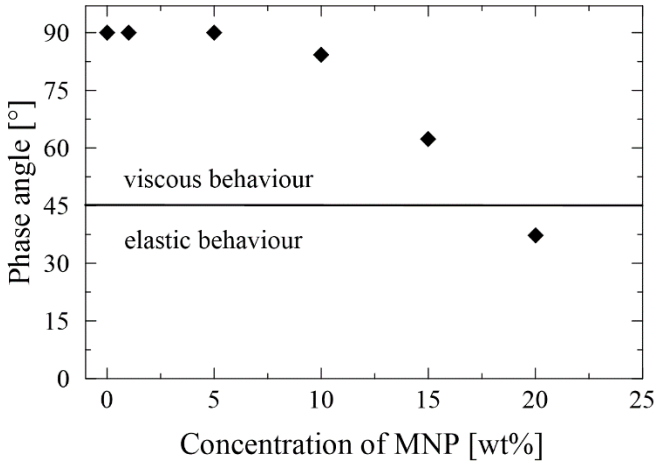

FIGURE 2 Effect of MNP concentration on the phase angle of the PVB/MNPs solutions (PVB 8 wt%) at the frequency of 1 Hz and strain of 1%.

Morphological and structural characterization of the membranes

The morphology of the nanofibrous membranes was determined by SEM. Initially, the effect of polymer concentration on fibre diameter was studied for neat PVB and PVB with a fixed amount of the MNPs (5 wt%), as shown in Figure 3a. In both cases, when polymer concentration was raised, the presence of beads disappeared and the diameters of the nanofibres increased. According to the literature, the expectation is that uniform circular nanofibres arise from PVB solutions of concentration exceeding 8 wt%.[27] Therefore, such a concentration was chosen for preparing magnetic nanofibrous membranes with different amounts of the MNPs (1–20 wt%). Subsequent SEM images for these (Figure 3b) revealed the morphological changes that occurred in the nanofibres alongside increase in MNP content. It was demonstrated that the highest concentration of the MNPs (20 wt%) significantly altered the structure of the nanofibres. Moreover, production of this nanofibrous membrane was slow and complicated in comparison with other concentrations, due to its high viscosity and elasticity (Figure 1b, Figure 2).

Figure 4 (a, b) details change in nanofibre diameter though manipulating PVB and MNP concentration, respectively. Raising the viscosity of the PVB solutions made the the fibres thicker, in general. It would seem that the act of heightening MNP content first led to increase in the diameters of the nanofibres but then this was seen to decrease as the viscosity of the PVB/MNPs solutions rose (Figure 3b). This was probably caused by the greater elasticity exhibited by the PVB solutions with a higher content of MNPs, confirmed by measurements of phase angle (Figure 2). A critical concentration of the MNPs was gauged at 10 wt%, the point at which the elasticity of the solutions began to intensify alongside concurrent drop in fibre diameter. In order to evaluate the statistical significance of change in fibre diameter through variance in MNP concentration, a one-way ANOVA test was applied in Minitab software. The *P*-value was equal to 0.000 with $1 - \alpha = 0.95$ and a probability of error of $\alpha = 5\%$; consequently, hypothesis H_0 derived as $\bar{x}_1 = \bar{x}_5 = \bar{x}_{10} = \bar{x}_{15} = \bar{x}_{20}$, where $\bar{x}_i$ represented the mean diameter of the fibre for given concentration *i* (1, 2, 5, 10 and 20 wt.%), was rejected in favour of an alternative hypothesis H_A: NON, which implied that the concentration of MNPs exerted a statistically significant effect on fibre diameter.

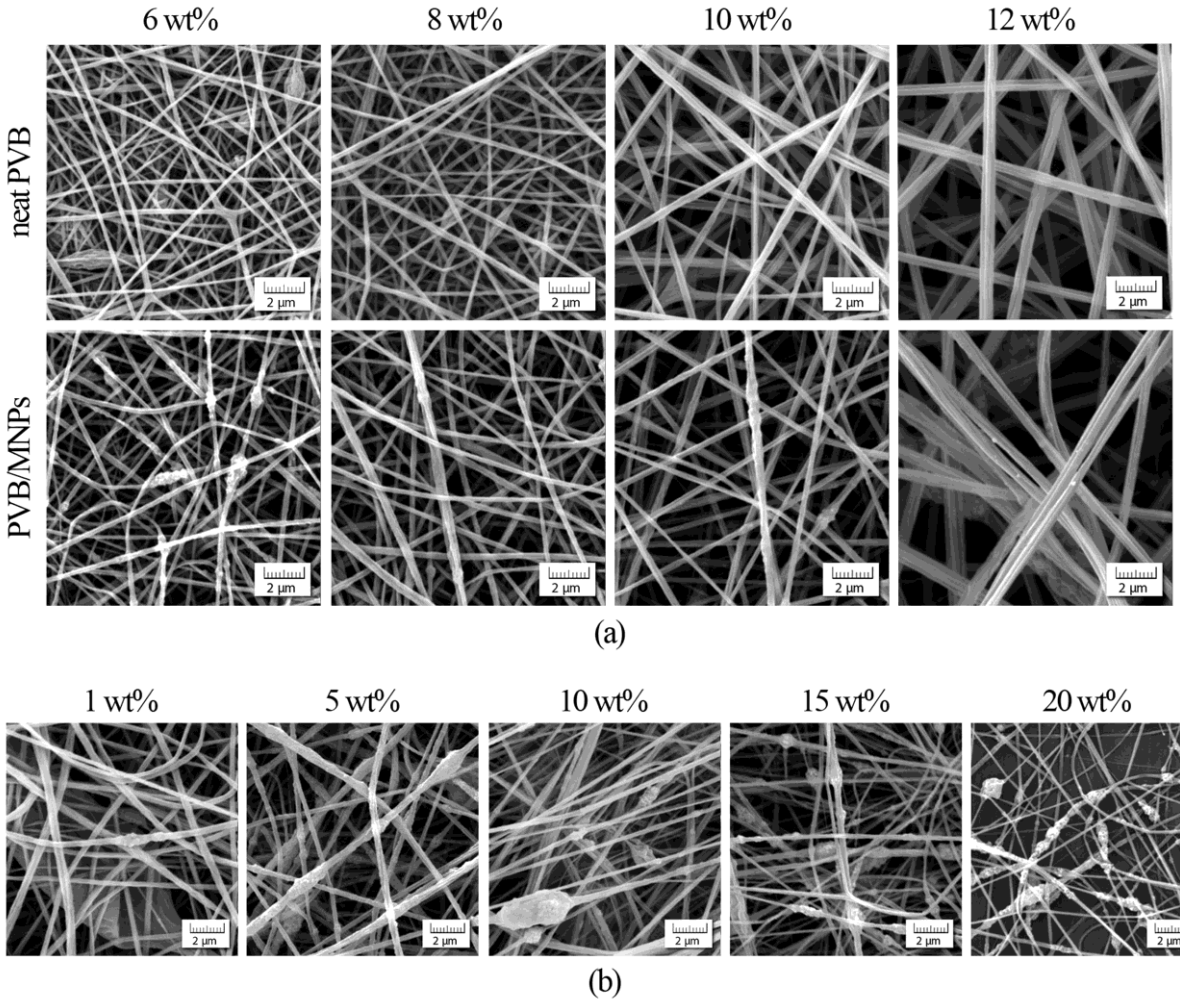

FIGURE 3 SEM images of: (a) neat PVB nanofibres and PVB/MNPs nanofibres with a fixed concentration of MNPs (5 wt%); (b) PVB/MNPs nanofibres with a fixed concentration of PVB (8 wt%).

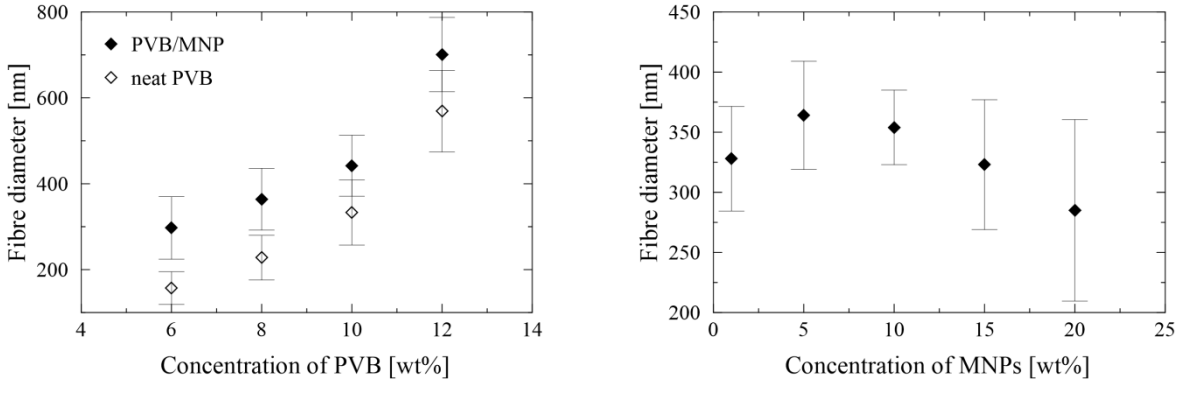

FIGURE 4 Dependence of fibre diameter on the concentration of: (a) neat PVB nanofibres and PVB/MNPs nanofibres with fixed MNP concentration (5 wt%); (b) PVB/MNPs nanofibres with fixed PVB concentration (8 wt%).

TEM analysis was employed for visualizing the MNPs embedded within the PVB nanofibres. Figure 5 shows TEM images of the PVB/MNPs nanofibres supplemented with different concentrations of the MNPs, the latter being spherical in shape with an approximate size of 30 nm. The extent to which the MNPs were incorporated into the polymer nanofibres was dependent on their concentration. It seems that the most homogeneous structure was obtained at the concentration of 10 wt% (MNPs). However, when the concentration of the MNPs was increased (above 15 wt%), particulate clusters were created that protruded from the nanofibres, thereby diminishing the porosity of the membrane.

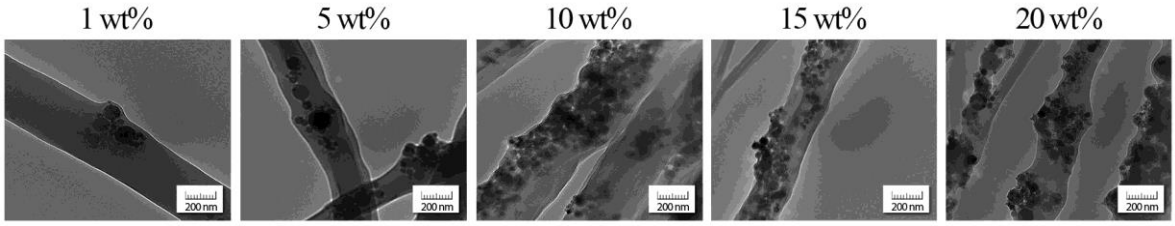

FIGURE 5 TEM images of the PVB nanofibres with progressive concentration of MNPs.

Nanofibres are formed during the electrospinning process upon drying of the electrically-charged jet of the polymer solution.[28] In the context of such drying, FTIR analysis was carried out to detect any potential residual methanol in the spun samples (the feedstock entries serving as a reference) as well as to neat PVB fibres and their PVB/MNPs composites. Figure 6 shows that the iron oxides did not exhibit any characteristic peaks in the studied region, apart from those attributable to the bending vibrations of absorbed water or surface hydroxyls.[29] The PVB granulate exhibited a broad absorption peak in the wavenumber range of 3 150 to 3 700 cm^{-1}, pertaining to the symmetrical stretching vibration of –OH groups in addition to the deformation mode at 1340 cm^{-1}.[30] The integrated area of the former peak, A3700–3150, was compared to those obtained for the neat PVB nanofibres and PVB/MNPs composites, respectively. This revealed that the area of the peak reduced (a decrease of 37%) after incorporating the MNPs, due to the lower relative content of PVB. More importantly, the A3700–3150 part of the curve was comparable to that for the neat PVB nanofibres (less than 10% difference), indicating that methanol had been successfully evaporated from the nanofibres when being streamed as a jet towards the collector.

Investigation was made as to any chemical interactions that occurred between the MNPs and PVB macromolecules. These generally comprised hydrogen bonding or dipolar interaction, manifested as shifts in bands and/or broadening of bands in the FTIR spectra of the composites [31]; comparing the relevant spectra in Figure 6 revealed the extent of such chemical interaction. The spectrum for neat PVB was almost identical to that reported in the literature, specifically the existence of peaks at 2 950 cm^{-1} and 2 870 cm^{-1}, characterizing the valence vibrations of CH_2 groups of the polymer backbone, as well as corresponding deformation modes at around 1 420 cm^{-1} and 1 380 cm^{-1}. [32] No sharp peak was discerned relating to C=O stretching vibrations of the acetate group, typically appearing at around 1 730 cm^{-1}, most probably due to very low content (1–4%) of vinyl acetate groups in the commercial PVB.[33] However, no significant differences in the spectra were visible, indicating that chemical interactions had not occurred between the MNPs and PVB during preparation of the solution in methanol.

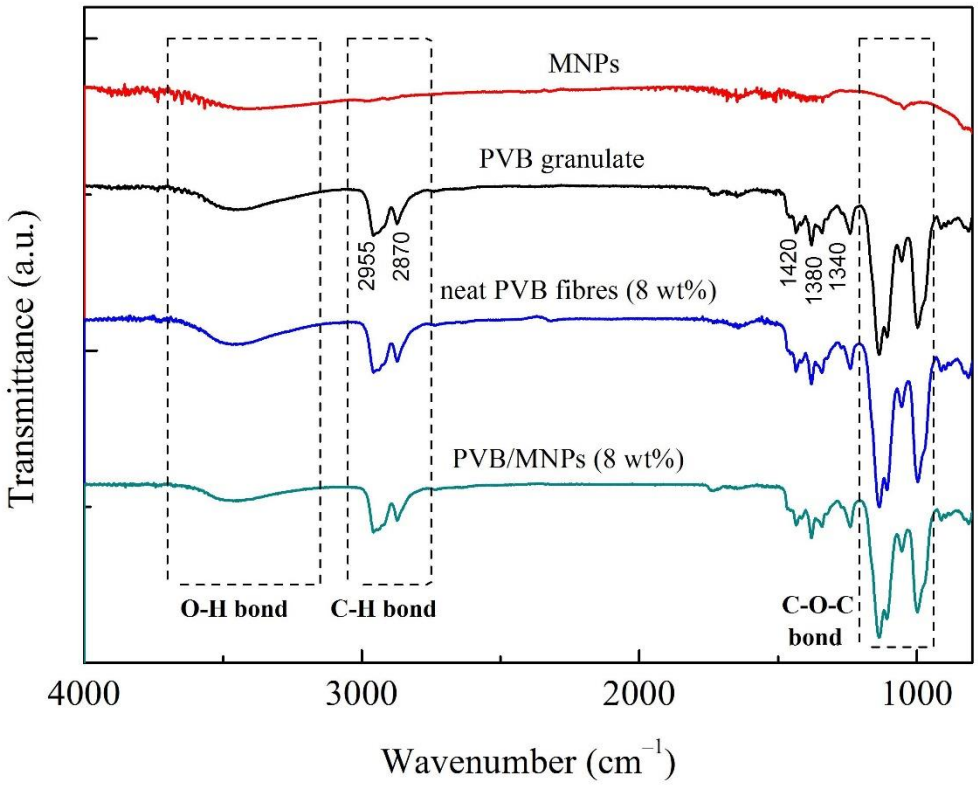

FIGURE 6 FTIR spectra for the feedstock entries, the electrospun PVB fibres (8 wt%) and their PVB/MNPs fibrous composites (8 wt%); the region of interest is demarcated in grey.

Magnetic properties of the membranes

As described earlier, exposing polymer-based nanofibres to a magnetic field means they can be variously utilized. To this end, the authors investigated the magnetic properties of the nanofibrous PVB/MNPs membranes by VSM. Figure 7 shows the mass magnetizations plotted versus the applied strength of the magnetic field, corresponding to the membranes prepared from methanol-based solutions of different PVB (a) and MNP (b) concentrations. The VSM recordings of the nanofibrous membranes exhibited thin yet open-loop characteristics, indicating ferromagnetic behaviour.[34] The corresponding coercive forces are displayed as the inset Figures. Increase in PVB concentration led to reduced saturation magnetization (MS) of the membranes - from 24.8 to 18.3 emu g^{-1} - for the MNPs at 5 wt%. In contrast, incorporating a different amount of the MNPs resulted in heightened MS values - from 6.4 to 45.5 emu g^{-1} – for the sample with a fixed PVB concentration of 8 wt%. These values were lower than for the neat MNPs (68 emu g^{-1}), due to the presence of a non-magnetic component (PVB), although they were still remarkably high for nanoparticulate systems. It is important to note that the residual magnetization was also quite high and increased in line with MNP content. Notably, the MS values for the electrospun PVB/MNPs membranes produced herein exceeded those of similar magnetic membranes reported in the literature.[8, 26, 35–37]

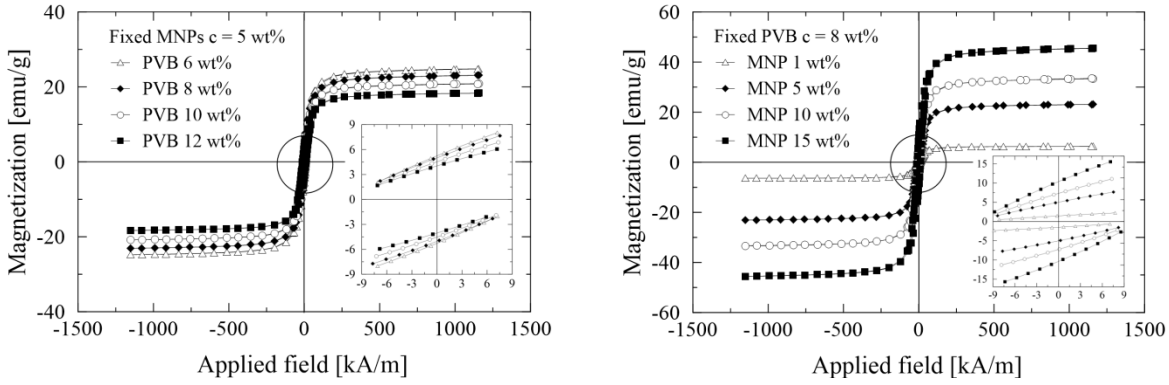

(**a**) (**b**)

FIGURE 7 Magnetic properties of: (a) PVB/MNPs nanofibres with fixed MNP concentration (5 wt%), (b) PVB/MNPs nanofibres with fixed PVB concentration (8 wt%).

At this point, it should be noted that the concentration of each component related to the feedstock solution prior to commencement of the electrospinning process. Assuming absolute evaporation of methanol takes place during the process at both the polymer jet and target collector, the true content of the magnetic filler (*MF*) can be determined by the following equation:

$$MF\ [\text{wt\%}] = \frac{M_S(membrane)}{M_S(MNPs)} \times 100 \quad , \qquad (5)$$

where M_S (membrane), and M_S (MNPs) are the saturation magnetizations of the membrane and neat MNPs, respectively.[28] As seen in Figure 8, MF values reached up to ca 67 wt%, explaining the remarkably high M_S of the PVB nanofibrous membranes. Verifying the data revealed that the calculated *MF* values were slightly lower than the MNP concentrations in the feedstock polymer solutions. A similar phenomenon was observed in the literature, further explained therein as a consequence of particle agglomeration and settling, due to a mismatch in density between the MNPs and polymer solution.[28]

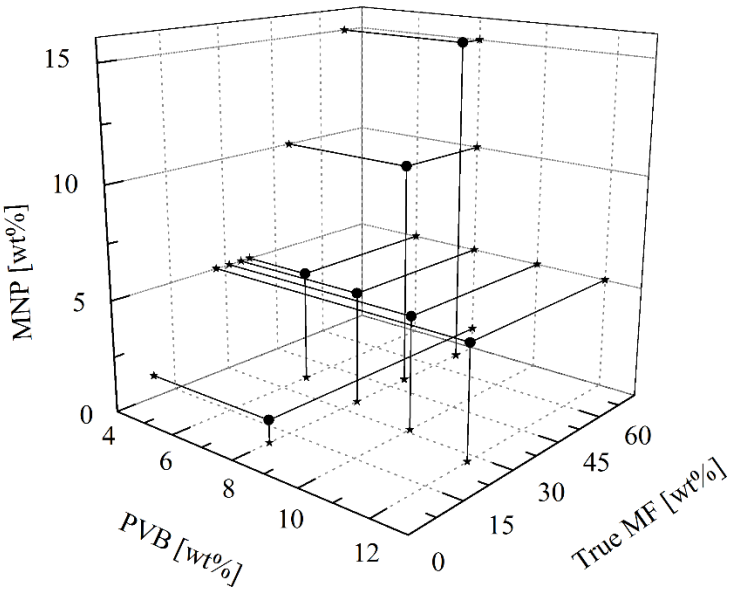

FIGURE 8 Representation of true MF in the PVB/MNPs nanofibres pertaining to the concentrations of MNPs and PVB in the feedstock solution.

Finally, the authors evaluated the magneto-mechanical responses of the PVB/MNPs nanofibres by analysing their VSM data. It was possible that the permeability of magnetic composites would experience remarkable features attributable to particles restructuring inside the matrix.[38] This hypothesis was later confirmed through direct microscopy observations and mathematical modelling.[39] The topic was later extended by investigating this phenomenon in magnetic elastomers, based on different extents of matrix stiffness under various temperatures.[40] Interestingly, research has recently been conducted elsewhere on magnetic elastomers with modified particle/matrix interaction.[41] Prior to the present study, though, field-induced restructuring of magnetic nanofibres had not been previously explored in this context. Figure 9 shows low-field magnetic susceptibility, plotted as a function of magnetic field strength, for the PVB nanofibrous membranes with various MNP concentrations. As is evident, the susceptibility of the membranes steeply increased after introducing a higher amount of the MNPs. Nevertheless, all the dependences exhibited local maxima of approximately ±14 kA m^{-1}, which proved such restructuring. A supposition to explain this is that the nanofibres in the membrane shifted into closer proximity with each other, so the distances traversed by the MNPs were shorter, thereby increasing magnetic susceptibility. After consulting studies dealing with other materials, it was noted that this process might also be accompanied by local field-induced orientation of the nanofibres along the magnetic flux lines.[39] Due to such remarkable behaviour, the PVB/MNPs nanofibrous membranes described herein may also, besides the intended application, find utilization as materials suitable for the magneto-mechanical stimulation of cells.[42]

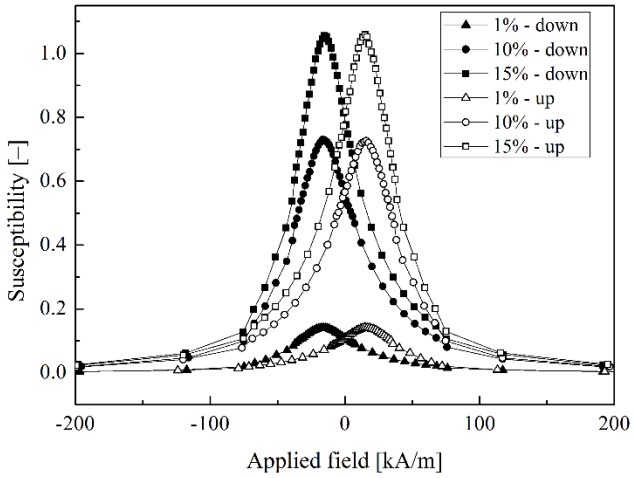

FIGURE 9 Low-field susceptibility of the PVB nanofibrous membranes containing different MNP concentrations as a function of decreasing (open symbols) and increasing (solid symbols) magnetic field strength.

Surface and filtration properties of the membranes

In order to analyse the wettability of the magnetic nanofibrous membranes, the authors determined the water contact angle (WCA) by the sessile drop method; average WCA values are given in Figure 10. As can be seen, all the PVB membranes exhibited hydrophobic properties in the range of 92° to 125°, while the neat PVB nanofibrous membranes exhibited WCAs exceeding 120°. A slight dependence in WCA values pertained to increase in fibre diameter (Figure 10a) and roughness as a result of higher PVB concentration. Nevertheless, a gradual drop in WCA was observed in parallel with rise in the concentration of the MNPs embedded inside the PVB nanofibres. Reduced WCAs imply better adhesion and filtration efficiency due to greater surface area existing between the nanofibres and water; this effect is consistent with a similar study.[43]

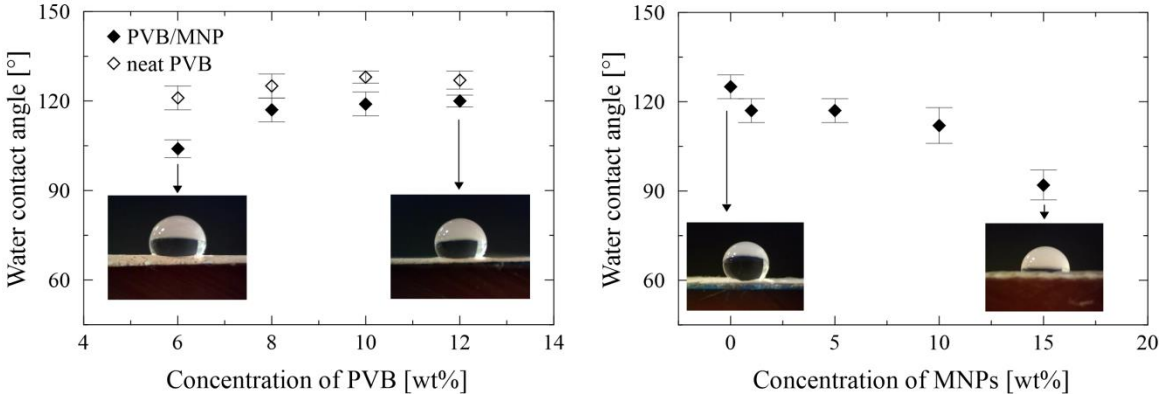

(**a**) (**b**)

FIGURE 10 Wettability of: (a) Neat PVB and PVB/MNPs nanofibres with fixed MNP concentration (5 wt%), (b) PVB/MNPs nanofibres with fixed PVB concentration (8 wt%).

A pilot filtration test was conducted on the PP non-woven textile in combination with the nanofibrous membrane (the latter at a set thickness of 20 μm) to evaluate the filtration properties of the system. The thickness of the nanofibrous layer constitutes a crucial parameter for determining total filtration efficiency, since permeation flux is inversely proportional to it.[19] The mean and maximum pore sizes of the final membranes are presented in Table 2, wherein pore size reduced in parallel with decrease in fibre diameter. The pore sizes of the neat PVB membranes were slightly lower than for those supplemented with the MNPs, potentially due to reduction in fibre-bonding points and expanded space between the fibres.[44] The change in permeation flux of the membranes was determined by dead-end cell filtration, which was influenced predominantly by fibre diameter and the presence of the MNPs (at a fixed concentration). Table 2 compares the morphological parameters with the filtration properties of the neat PVB and PVB/MNPs nanofibrous membranes. In agreement with the literature, the membranes with thicker fibre diameter (above 570 nm) exhibited excellent water permeation flux.[43,45] Where MNPs had been incorporated, extensive decrease in permeation flux was observed independent of fibre diameter. This may have been caused by the increased roughness and lower porosity of the PVB/MNPs membranes in combination with water flow instability during filtration. The low porosity of the membranes possibly arose as a consequence of the total thickness of filter, this consisting of the PP non-woven textile and the electrospun nanofibrous membrane, which was in good agreement with results obtained.[46] The reduction in WCA for the membranes exerted a minimal effect in correlation with permeation flux. In all cases, the permeation flux of the model solution was lower than for pure water due to the presence of the iron ions and their capture by the membrane.

TABLE 2 Mean and maximum pore sizes, porosity, permeation flux and filtration efficiency of selected neat PVB and PVB/MNPs samples with a fixed concentration of MNPs in the nanofibrous membranes.

Sample code	**Mean pore size [μm]**	**Max. pore size [μm]**	**Porosity [%]**	**Flux**$_{(water)}$ **[L m^{-2} h^{-1}]**	**Flux**$_{(model\ solution)}$ **[L m^{-2} h^{-1}]**	**Filtration efficiency [%]**
PVB8	0.44±0.14	0.65	39±4	750±20	530±10	43±10
PVB8/MNP5	0.56±0.17	0.98	19±1	440±10	390±10	81±6
PVB10	0.79±0.25	1.00	29±3	1 450±150	1 180±10	66±8
PVB10/MNP5	0.99 ±0.30	1.10	17±2	1 120±100	950±10	88±10
PVB12	1.02±0.22	1.60	28±1	75 550±660	63 690±600	14±4
PVB12/MNP5	1.35±0.47	1.85	18±2	42 520±720	39 580±690	22±4

The filtration efficiency (*FE*) for all the membranes tested for removing metal ions from the model solution was calculated from the concentration of solutions before and after filtration took place (Table 2). The membranes containing the MNPs were highly efficient at removing the iron ions from water, in comparison with their neat PVB analogues; the PVB10/MNP5 sample showed the highest efficiency of 88%. Similar results were obtained for nanofibrous membranes based on polyethylenimine/polyacrylonitril/Fe_3O_4, which demonstrated a filtration efficiency of over 98.5% at the

flux rate of 765 l m^{-2} h^{-1} (at an applied pressure of 0.2 bar).[19] The exception was the PVB12/MNP5 membrane, for which permeation flux and mean pore size were considerably high, causing higher working pressure; the metal ions most likely drifted away in this instance, resulting in reduced *FE*. Based on these results, it can be deduced that the presence of the MNPs increased the value of *FE*, despite the magnetic membranes possessing greater fibre diameters. This indicates that the MNPs actively contributed to enhancing *FE* (without the external magnetic field) as per removal of the Fe(III) ions. The adsorption mechanism presumably transpired through the lower hydrophobicity of the metal surface, thus more oxygen-containing surface groups existed with ion-exchange properties.[21] The rough surface structure of the PVB10/MNP5 sample could have enhanced contact between the Fe(III) ions and the fibres during the filtration process, this constituting a complex mechanism of mechanical retention and active iron bonding. In future work, investigating presence of an external magnetic field during the filtration might prove important.

CONCLUSIONS

Neat PVB and PVB/MNPs nanofibrous membranes were successfully prepared via electrospinning. The effects of the concentration of the PVB and MNPs on the functional behaviour of the membranes were thoroughly investigated and compared. From the rheological properties of the solutions, the critical concentration of the MNPs (15 wt%) in the PVB solution was deduced and high quality nanofibrous membranes were produced. Incorporating a higher amount of the MNPs in the PVB membrane gave rise to greater surface wettability (a drop in WCA ca 30°) and magnetic performance. The PVB/MNPs membranes exhibited ferromagnetic behaviour, with saturation magnetizations reaching up to 45.5 emu g^{-1}. Susceptibility measurements revealed the field-induced motions of the MNPs in the body of the membranes, which was further explained as a consequence of the nanofibres undergoing restructuring, accompanied by local elongation. A broad series of fabricated membranes underwent analysis, with the aim of discerning the most promising one for practical application. The most efficient magnetic membrane in terms of filtration was seen to be the formulation PVB10/MNP5, which exhibited high water flux (1 120±100 l m^{-2} h^{-1}) and remarkable filtration efficiency (88±10%) with moderate magnetic saturation (20 emu g^{-1}). Using this membrane, the concentration of iron ions in the model solution decreased from 5 mg l^{-1} to only 0.6 mg l^{-1}. This particular membrane shows potential for employment as a key component in the water treatment process.

ACKNOWLEDGEMENTS

This research was supported by the Ministry of Education, Youth and Sports of the Czech Republic (Project LTC 19034), and within Program NPU I (LO1504). Institutional support was provided by the Czech Academy of Sciences, Czech Republic (RVO: 67985874). This work was also carried out under the framework of COST Actions CA17107. M.C and M.S wish to thank the Czech Science Foundation (17-24730S) for its financial support.

REFERENCES AND NOTES

1. Singh, R. K.; Patel, K. D.; Lee, J. H.; Lee, E. J. *PLoS One* **2014***, 9,* e91584

2. Fallahiarezoudar, E.; Ahmadipourroudposht, M.; Yusof, N. M; Idris, A.; Ngadiman, N. H. A. *Polymers* **2017**, *9*, 584.
3. Mortimer, C. J.; Wright, C. J. *Biotechnol. J.* **2017**, *12*, 1600693.
4. Liang, F. C.; Luo, Y. L.; Kuo, C. C.; Chen, B. Y.; Cho, C. J.; Lin, F. J.; Yu, Y. Y.; Borsali, R. *Polymers* **2017**, *9*, 136.
5. Cai, N.; Li, C.; Han, C.; Luo, X.; Shen, L.; Xue, Y.; Yu, F. Q. *Appl. Surf. Sci.* **2016**, *369*, 492–500.
6. Zhong, Y.; Leung, V.; Wan, L. Y.; Dutz, S.; Ko, F. K.; Hafeli, U. O. *J. Magn. Magn. Mater*. **2014**, *380*, 330.
7. Peter, K. T.; Myung, N. V.; Cwiettny, D. M. *Environ. Sci. Nano*. **2018**, *5*, 669.
8. Savva, I.; Constantinou, D.; Marinica, O.; Vasile, E.; Vekas, L.; Krasia-Christoforou, T. *J. Magn. Magn. Mater.* **2014**, *352*, 30.
9. Prochazkova, J.; Pospiskova, K.; Safarik, I. *J. Magn. Magn. Mater.* **2019**, *473*, 335.
10. Faridi-Majidi, F.; Sharifi-Sanjani, N. *J. Appl. Polym. Sci.* **2007**, *105*, 1351.
11. Ray, S. S.; Chen, S. S.; Li, C. W.; Nguyen, N. C.; Nguyen, H. T. *RSC Adv.* **2016**, *6*, 85495.
12. Shahkaramipour, N.; Tran, T.N.; Ramanan, S.; Lin, H. *Membranes* **2017**, *7*, 7010013.
13. Zhu, M.; Han, J.; Wang, F.; Shao, W.; Xiong, R.; Zhang, Q.; Pan, H.; Yang, Y.; Samal, S. K.; Zhang, F.; Huang, C. *Macromol. Mater. Eng.* **2017**, *302*, 1600353.
14. Ahn, B. W.; Kang, T. J. *J. Appl. Polym. Sci.* **2012**, *125*, 1567.
15. Nasir, A. M.; Goh, P. S.; Abdullah, M. S.; Ng, B. C. Ismail, A. F. *Chemosphere*, **2019**, *232*, 96.
16. Nasreen, S. A. A. N.; Sundarrajan, S.; Nizar, S. A. S.; Balamurugan, R.; Ramakrishna, S. *Membranes* **2013**, *3*, 266.
17. Jiang, Z.; Tijing, L. D.; Amarjargal, A.; Park, G. H.; An, K. J.; Shon, H. K.; Kim, C. S. *Composites, Part B* **2017**, *77*, 311.
18. EL-Rafei, A. M.; El-Kalliny, A. S.; Gad-Allah, T. A. *J. Magn. Magn. Mater*. **2017**, *428*, 92.
19. Zhao, R.; Li, X.; Li, Y.; Li, Y.; Sun, B.; Zhang, N.; Chao, S.; Wang, C. *J. Colloid Interface Sci.* **2017**, *505*, 1018.
20. Bordoli, S.; Nath, S. K; Dutta, R. K. *Desalination* **2011**, *281*, 190.
21. McCord, J. M. *Nutr. Rev.* **1996**, *54*, 85.
22. Kaveeshwar, A. R.; Ponnusamy, S. K.; Revellame, E. D.; Gang, D. D.; Zappi, M. E.; Subramaniam, R. *Process Saf. Environ. Prot.* **2018**, *114*, 107.
23. Goetz, L. A.; Jalvo, B.; Rosal, R.; Mathew, A. P. *J. Membr. Sci.* **2016**, *510*, 238.
24. Cascone, E.; David, D. J.; Di Lorenzo, M. L.; Karasz, F. E.; Macknight, W. J.; Martuscelli, E.; Raimo, M. *J. Appl. Polym. Sci.* **2001**, 82, 2934.
25. Rosic, R.; Pelipenko, J.; Kocbek, P.; Baumgartner, S.; Bester-Rogac, M; Kristl, J. *Eur. Polym. J.* **2012**, *48*, 1374.
26. Zhang, D.; Karki, A. B.; Rutman, D.; Young, D. P.; Wang, A.; Cocke, D.; Ho, T. H.; Guo, Z. H. *Polymer* **2009**, *50*, 4189.
27. Peer, P.; Polaskova, M.; Suly, P. *Chinese J. Polym. Sci.* **2018**, *36*, 742.
28. Brito-Pereira, R.; Correia, D. M.; Ribeiro, C.; Francesko, A.; Etxebarria, I.; Perez-Alvarez, L.; Vilas, J. L.; Martins, P.; Lanceros-Mendez, S. *Composites, Part B* **2018**, *141*, 70.
29. Zhang, S.; Wu, W.; Xiao, X.; Zhou, J.; Ren, F.; Jiang, C. *Nanoscale Res. Lett.* **2011**, *6*, 89.
30. Bai, Y.; Chen, Y.; Wang, Q.; Wang, T. *J. Mater. Chem. A* **2014**, *2*, 9169.

31. Bulbul, Y. E.; Eskitoros-Togay, S. M.; Demirtas-Korkmaz, F.; Dilsiz, N. *Int. J. Pharm.* **2019**, 568, 115813.
32. Yang, H.; Dai, J.; Liu, X.; Lin, Y.; Wang, F.; Liu, P. *J. Alloys Compd*. **2017**, *714*, 537.
33. Lian, F.; Wen, Y.; Ren, Y.; Guan, H. Y. J. Membr. Sci. 2014, 456, 42.
34. Palchoudhury, S.; An, W.; Xu, Y.; Qin, Y.; Zhang, Z.; Chopra, N.; Holler, R. A.; Turner, C. H.; Bao, Y. P. *Nano Lett.* **2011**, *11*, 1141.
35. Wang, S.; Wang, C.; Zhang, B.; Sun, Z.; Li, Z.; Jiang, X.; Bai, X. D. *Mater. Lett.* **2010**, *64*, 9.
36. Wang, H.; Li, Y.; Sun, L.; Li, Y.; Wang, W.; Wang, S. A.; Xu, S. F.; Yang, Q. B. *J. Colloid Interface Sci.* **2010**, *350*, 396.
37. Kim, J.; Hong, S. C.; Bae, G. N.; Jung, J. H. *Environ. Sci. Technol.* **2017**, *51*, 11967.
38. de Vicente, J.; Bossis, G.; Lacis, S.; Guyot, M. *J. Magn. Magn. Mater.* **2002**, *251*, 100.
39. Stepanov, G. V.; Borin, D. Y.; Raikher, Y. L.; Melenev, P. V.; Perov, N. S. *J. Physics: Condens. Matter.* **2008**, *20*, 494216.
40. Bodnaruk, A. V.; Brunhuber, A.; Kalita, V. M.; Kulyk, M. M.; Snarskii, A. A.; Lozenko, A. F.; Ryabchenko, S.; Shamonin, M. *J. Appl. Phys.* **2018**, *123*, 115118.
41. Cvek, M.; Mrlik, M.; Sevcik, J.; Sedlacik, M. *Polymers* **2018**, *10*, 1411.
42. Ribeiro, C.; Correia, V.; Martins, P.; Gama, F. M.; Lanceros-Mendez, S. *Colloids Surf. B* **2016**, *140*, 430.
43. Liu, S.; Li, L.; Liu, R.; Liu, J.; Zhao, X.; Liao, X. *J. Phys. D: Appl. Phys.* **2020**, 53, 195403.
44. Deng, S.; Liu, X.; Liao, J.; Lin, H.; Liu, F. *Chem. Eng. J.* **2019**, *375*, 122086.
45. Al-Attabi, R.; Rodrigues-Andres, J.; Schutz, J.A.; Bechelany, M.; des Ligneris, E.; Chen, X.; Kong, L.; Morsi, Y. S.; Dumee, L. F. *Sep. Purif. Technol*. **2019**, *229*, 115806.
46. Liu, Z. Y.; Wei, Z. M.; Wang, X. J.; Zhang, G.; Long, S. R.; Yang, J. *Chinese J Polym. Sci*. **2019**, *37*, 1248.